# Predictions of birefringence and dichroism of hard sphere suspensions in combined electric and shear fields

Paul M. Adriani and Alice P. Gast

Citation: The Journal of Chemical Physics **91**, 6282 (1989); doi: 10.1063/1.457394
View online: http://dx.doi.org/10.1063/1.457394
View Table of Contents: http://scitation.aip.org/content/aip/journal/jcp/91/10?ver=pdfcov
Published by the AIP Publishing

# Predictions of birefringence and dichroism of hard sphere suspensions in combined electric and shear fields

Paul M. Adriani and Alice P. Gast
*Department of Chemical Engineering, Stanford University, Stanford, California 94305-5025*

(Received 15 May 1989; accepted 8 August 1989)

We present the optical anisotropy of a hard sphere suspension subjected to combined electric and shear fields. We model the particle structure factor as a shear induced perturbation of the anisotropic structure induced by electric field. We renormalize the nonconvergent birefringence integral to allow calculation of birefrigence from the particle structure factor. The principle axes of the birefringence and dichroism tensors vary with the Mason number, a measure of the relative strength of shear forces to electric dipole interaction forces. The principle axes only coincide in the shear dominated and the electric field dominated limits. The magnitudes of birefringence and dichroism are sensitive to the particle size relative to the wave-length of light employed. We compare theoretical predictions in the limit of pure shear to the experiments of Wagner *et al.*, J. Chem. Phys. **89**, 1580 (1988), employing a simple affine deformation theory for the structure factor, which yields fair agreement with experiment for the dichroism but poor agreement for the birefringence. The prediction of optical properties provides both a test for theories of microstructure and insight into the effects of shear and electric fields on microstructure.

## I. INTRODUCTION

Suspensions of colloidal particles exhibit substantial changes in particle distribution when subjected to applied shear,[1] electric,[2] or magnetic[3] fields. These microstructural changes affect bulk transport properties and a variety of rheological properties including the storage and loss modulus of oscillatory flow[2] and the shear viscosity.[1] For electric fields, possible applications include a variety of electrically controlled vibration dissipation and antishock devices.[4]

Studies of suspension microstructure under applied fields are interesting in their own right and contribute to an understanding of the way applied fields affect bulk properties, often calculated theoretically from integrals over the particle microstructure. Light scattering studies such as those by Ackerson *et al.*[5,6] determine the particle structure factor over a limited range of scattering vectors. Birefringence and linear dichroism are useful experimental probes for studying the static and dynamic structure of colloidal suspensions under applied fields.[7] Birefringence and dichroism are measures of the anisotropy in the index of refraction and the attenuation, respectively. These optical experiments allow noninvasive transient structural measurements, the primary experimental requirement being that concentrated suspensions comprise particles and solvent having similar indices of refraction to minimize turbidity.

The birefringence and dichroism of a medium with a known, weakly fluctuating index of refraction can be calculated via the theory of Onuki and Doi.[8] However, Onuki and Doi's expression for the birefringence is not always convergent; in the present problem we must renormalize the birefringence integral.

In this paper we consider a suspension of dielectric spheres in a dielectric liquid subjected to combined electric and shear fields. In a mean field approximation each sphere is equally polarized by the applied electric field. We model the particles as hard spheres with identical, aligned point dipoles, neglecting higher multipole interactions. The anisotropic dipolar interaction yields an anisotropic particle structure. Shear flow also produces an anisotropic particle pair distribution through the simultaneous strain and rotation of the microstructure. The shear-induced anisotropy is of dipole symmetry, anologous to the electric dipole anisotropy, permitting the two effects to be calculated similarly. From these model structure factors we calculate birefringence and dichroism. The birefringence calculation is not straightforward due to a nonconvergent integral. We derive a renormalization of this birefringence integral and then present theoretical predictions of birefringence and dichroism.

## II. INTERACTION ENERGY AND EQUILIBRIUM PAIR DISTRIBUTION FUNCTION

The potential energy of interaction $w(r,\theta)$ between two hard spheres with aligned point dipoles of dipole moment $\mu$ in a medium of dielectric constant $\epsilon_1$ is

$$\frac{w(r,\theta)}{kT}=\begin{cases}\infty, & \dfrac{r}{2a}<1\\ -\dfrac{2\Lambda}{(r/2a)^3}P_2(\cos\theta), & \dfrac{r}{2a}\geqslant 1\end{cases}, \tag{1}$$

where $kT$ is the thermal energy, $r$ is the distance between the dipoles, $a$ is the particle radius, $\theta$ is the angle between the dipole moment vector and the center-to-center vector $\mathbf{r}$, $P_2(x)=(3x^2-1)/2$ is the second Legendre polynomial, and $\Lambda=\mu^2/8a^3\epsilon_1 kT$ is a dimensionless dipole interaction strength. A diagram of our coordinate system and the geometry of the electric field in Fig. 1 shows the dipole moments aligned with the electric field along the $z$ axis.

We determine the distribution of the polarized spheres

 0021-9606/89/226282-08$02.10 

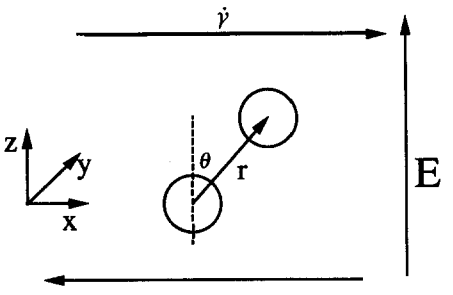


FIG. 1. Geometry of a particle pair where $r$ is the distance between the centers of the spheres, $\theta$ is the angle between $z$ and the center-to-center vector, the electric field vector $\mathbf{E}$ is in the $z$ direction and the shear rate $\dot{\gamma}$ is in the $x$ direction.

via the equilibrium particle pair distribution $g_{eq}(r,\theta)$ of hard spheres with aligned, rigid dipoles. This normalized pair distribution function relates the local particle density to the bulk density via $\rho(r,\theta) = \rho g(r,\theta)$. Hayter and Pynn[3] derived an expression for the pair distribution function by employing the mean spherical approximation (MSA) closure for the Ornstein–Zernike equation and by expanding the distribution function in Legendre polynomials to yield

$$g_{eq}(r,\theta) = g_0(r) + h_2(r)P_2(\cos\theta)\,, \tag{2}$$

where $g_0(r)$ and $h_2(r)$ depend on particle volume fraction $\phi$ and the dipole interaction strength $\Lambda$. Equation, (2) describes the structure in concentrated suspensions of aligned magnetic dipoles quite accurately.[9]

The scattering structure factor, obtained via a three dimensional Fourier transform of this particle pair distribution, is[3]

$$S(\mathbf{q}) = 1 + \rho h_0(q) + \rho h_2(q)(3\cos^2\phi' - 1)/2\,, \tag{3}$$

where $\mathbf{q}$ is the scattering vector, $\phi'$ is the angle between the scattering vector and the applied electric field, $q = (4\pi n/\lambda)\sin(\theta'/2)$, $n$ is the index of refraction of the suspension, $\lambda$ is the wavelength of the light in vacuum, $\theta'$ is the scattering angle, $h_0(q)$ is the Hankel transform of $g_0(r) - 1$, $h_2(q)$ is the Hankel transform of $h_2(r)$, and the Hankel transform pair is defined as[3]

$$f(q) = 4\pi\int_0^\infty j_2(qr)r^2 f(r)dr \tag{4}$$

and

$$f(r) = -\frac{1}{2\pi^2}\int_0^\infty j_2(qr)q^2 f(q)dq\,,$$

where

$$j_2(x) = \left(\frac{3}{x^3} - \frac{1}{x}\right)\sin x - \frac{3}{x^2}\cos x$$

is the second spherical Bessel function.

In a suspension of spheres with dielectric constant $\epsilon_2$, the dipole strength of each sphere can be determined in a self-consistent mean field approximation[2] as

$$\mu = \mu_0/\left\{1 - \beta\phi - \frac{6\beta\phi}{4\pi}\int_{2a}^\infty \frac{P_2(\cos\theta)}{r^3}[g(\mathbf{r}) - 1]d\mathbf{r}\right\}, \tag{5}$$

where $\phi = 4\pi\rho a^3/3$ is the particle volume fraction, $\beta = (\epsilon_2 - \epsilon_1)/(\epsilon_2 + 2\epsilon_1)$, and $\mu_0 = \epsilon_1\beta a^3 E$ is the dipole moment of an isolated sphere. Equation (5) must be solved self-consistently with Eq. (2) since the particle pair distribution depends on the strength of the dipole moment.

Substitution of the mean spherical approximation for the equilibrium particle pair distribution from Eq. (2) into Eq. (5) and angular integration using the orthogonality properties of Legendre polynomials yields

$$\Lambda = \Lambda_0/\left(1 - \beta\phi - \tfrac{6}{5}\beta\phi\int_{2a}^\infty \frac{1}{r}h_2\,dr\right)^2, \tag{6}$$

where $\Lambda_0 = \mu_0^2/8a^3\epsilon_1 kT$ is the dipole interaction strength in the dilute limit. The integral in Eq. (6) is given by Hayter and Pynn[3] as an implicit analytic expression dependent on the mean field dipole strength $\Lambda$. A simple iterative calculation determines $\Lambda$ for given volume fraction, isolated dipole strength $\Lambda_0$, and dielectric constants, $\epsilon_1$ and $\epsilon_2$. As $\beta$ and $\phi$ increase, the effective dipole moment increases. Now with Eq. (6) we have a means of solving the equilibrium structure as a function of the material properties ($\beta$ and $\epsilon_1$), volume fraction $\phi$, and the applied potential gradient $\mathbf{E}$.

## III. PAIR DISTRIBUTION AND STRUCTURE FACTOR IN SIMPLE SHEAR FLOW

Under steady shear flow the particle distribution is distorted from equilibrium, albeit a small perturbation for weak flows. We perturb $g_{eq}(r,\theta)$ with an affine deformation to yield

$$g(\mathbf{r}) = g_{eq}(r,\theta) + h_+(r,\theta)\left(\frac{xz}{r^2}\right), \tag{7}$$

where

$$h_+(r,\theta) = -\mathrm{Pe}\left[r\frac{\partial g_{eq}(r,\theta)}{\partial r} - \frac{\cos\theta}{\sin\theta}\frac{\partial g_{eq}(r,\theta)}{\partial\theta}\right], \tag{8}$$

the Peclet number is $\mathrm{Pe} = 3\pi\eta_0 a^3\dot{\gamma}/kT$, $\eta_0$ is the solvent viscosity, and $\dot{\gamma}$ is the shear rate. This equation describes an affine deformation induced by the shear and a Brownian relaxation toward equilibrium with the magnitude of the perturbation governed by the Peclet number. Substituting Eq. (2) for $g_{eq}(r,\theta)$ yields

$$h_+(r,\theta) = -\mathrm{Pe}\left\{\left[r\frac{dg_0(r)}{dr} + h_2(r)\right] + \left[r\frac{dh_2(r)}{dr} + 2h_2(r)\right]P_2(\cos\theta)\right\}. \tag{9}$$

Assuming affine deformation has the virtue of simplicity, but neglects hydrodynamic interactions and is not satisfactory on small length scales where hard spheres must avoid interpenetration. More complex theories of the pair distribution under steady shear[10,11] include approximate hydrodynamic interactions and account for hard sphere impenetrability, but are difficult to use and are not yet wholly satisfactory.

We Fourier transform Eq. (7) to find the scattering structure factor:

$$S(\mathbf{q}) = 1 + \rho h_0(q) + \rho h_2(q) P_2(\cos\phi') + \rho F_3\left[h_+(r,\theta)\frac{xz}{r^2}\right], \quad (10)$$

where the last term is the three-dimensional Fourier transform of the shear induced structure. To simplify the equations for birefringe and dichroism, and clarify how they vary as the microstructure changes from electric dominated to shear dominated, we expand $S(\mathbf{q})$ to first order in Pe and $\Lambda$ to give

$$h_0(q) = h_{HS}(q) + \Lambda h_\alpha(q) + O(\Lambda^2),$$
$$h_2(q) = \Lambda h_{2\alpha}(q) + O(\Lambda^2),$$

and

$$F_3\left[h_+(r,\theta)\frac{xz}{r^2}\right] = h_+(q)\left(\frac{q_x q_z}{q^2}\right) + O(\mathrm{Pe}\,\Lambda), \quad (11)$$

where

$$h_+(q) = -\mathrm{Pe}\, q\frac{dh_{\mathrm{HS}}(q)}{dq}, \quad (12)$$

where $h_{\mathrm{HS}}(q)$ is the transform of the hard sphere total correlation function, and the subscript $\alpha$ denotes the terms that are the first order in $\Lambda$. The expression for $h_+$ in Eq. (12) corresponds to the affine deformation of the hard sphere structure.[12]

The relative magnitude of the shear and electric forces perturbing the isotropic particle pair distribution can be gauged by the Mason number

$$\mathrm{Mn} = \mathrm{Pe}/\Lambda, \quad (13)$$

the ratio of the Peclet number to the dipole interaction strength. This ratio is called the Mason number[13] in honor of the contributions of Mason to the study of particles subjected to shear and electric fields. In the following sections, the Mason number will be a key parameter for the prediction of optical properties from the structure factors given by Eqs. (4) and (10).

## IV. DIELECTRIC TENSOR

The theory of Onuki and Doi[8] relates the birefringence and dichroism of a polymer solution to fluctuations in polymer concentration. Our summary of their theory applied to colloidal suspensions follows Wagner *et al*[7] and uses their notation. Beginning with the assumption of a medium with a weakly fluctuating dielectric constant, Onuki and Doi derive a perturbation solution of Maxwell's equations yielding the ensemble average of the dielectric tensor in terms of the distribution of fluctuations. Anisotropy in fluctuations produces an anisotropic dielectric tensor which in turn causes birefringence and dichroism. Onuki and Doi's result for the dielectric tensor is

$$\epsilon = -\frac{\epsilon A}{(2\pi)^3}\left(\frac{4\pi a^3}{3}\right)^2 \int d\mathbf{q} C(\mathbf{k}-\mathbf{q})\left(\frac{\mathbf{qq} - k^2\delta}{q^2 - k^2}\right) + \mathrm{I.T.} \quad (14)$$

with

$$C(\mathbf{q}) = \int d\mathbf{r}\, e^{-i\mathbf{q}\cdot\mathbf{r}}\langle\delta\rho(\mathbf{0})\delta\rho(\mathbf{r})\rangle, \quad (15)$$

and

$$A = \left(\frac{1}{\epsilon}\frac{d\epsilon}{d\phi}\right)^2, \quad (16)$$

where $\epsilon$ is the dielectric constant of the isotropic suspension without applied electric or shear fields, $\mathbf{k}$ is the wave vector of the light, $k = 2\pi n/\lambda$, $\mathbf{q}$ is the scattering vector, $q = 2k\sin(\theta'/2)$, I.T. stands for isotropic terms, $C(\mathbf{q})$ is the structure factor of the concentration fluctuations $\delta\rho$, and $A$ is a material property determined experimentally from the turbidity.[7,8]

If the structure factor is of form

$$C(\mathbf{q}) = C_0(q) - \frac{\mathbf{q}\cdot C_1(q)\cdot\mathbf{q}}{q^2}, \quad (17)$$

then the dielectric tensor simplifies to

$$\epsilon = \frac{\epsilon A}{16\pi^2}\left(\frac{4\pi a^3}{3}\right)^2 \int_0^\infty dq\, q^2 \Psi_b\left(\frac{q}{2k}\right) C_1(q) + \mathrm{I.T.}, \quad (18)$$

where $\Psi_b$ is a complex function[8] whose real and imaginary parts yield the birefringence and the dichroism, respectively. The above results can be applied to colloidal suspensions by relating the fluctuations in concentration to the particle pair distribution. The relation, derived by Wagner *et al.*,[7] is

$$\rho^2[g(\mathbf{r}) - 1] = \langle\delta\rho(\mathbf{0})\delta\rho(\mathbf{r})\rangle. \quad (19)$$

Substitution of Eq. (19) into Eq. (15) shows that the structure factor of the concentration fluctuations can also be determined from the structure factor of the particle distribution.

For both the MSA solution of aligned dipolar hard spheres and the pair distribution under simple shear, the form of Eq. (17) holds when we relate the anisotropic part of the structure factor to the anisotropic part of the particle pair distribution, as

$$C_1(q) = \frac{1}{2}\begin{pmatrix}1 & 0 & 0\\ 0 & 1 & 0\\ 0 & 0 & -2\end{pmatrix}\rho^2 h_2(q) + \frac{1}{2}\begin{pmatrix}0 & 0 & 1\\ 0 & 0 & 0\\ 1 & 0 & 0\end{pmatrix}\rho^2 h_+(q), \quad (20)$$

where the first term due to the electric field has principal axes aligned in $x$,$y$, and $z$ directions, while the second term due to the shear flow has principal axes in the $y$ direction and at 45° and 135° in the $xz$ plane. The principal axes of $C_1$ will vary with the relative importance of the two fields. However, substitution of Eq. (20) into Eq. (18) does not immediately yield a useful expression for the dielectric tensor of a hard sphere suspension since at large $q$,

$$h_1(q) = -4\pi(2a)^3 h_i(r = 2a)\frac{\cos(2qa)}{(2qa)^2} + O(1/q^3)$$

and

$$\mathrm{Re}[\Psi_b(q)] = 16/15 + O(1/q^2),$$

where subscript $i = +$ or 2 for the shear and electric fields respectively, making the real part of the integral nonconvergent. The large $q$ behavior of the structure factor is deter-

mined by the jump discontinuity in the pair distribution due to the excluded volume of each sphere, so this feature of the structures factor is similar for both the electric and the shear-induced structure. To renormalize this integral, we first separate Eq. (18) into convergent and nonconvergent parts

$$\int_0^\infty dq\, q^2 \Psi_b\left(\frac{q}{2k}\right) C_1(q) = \int_0^\infty dq\, q^2 \left[\Psi_b\left(\frac{q}{2k}\right) - \frac{16}{15}\right] C_1(q) + \frac{16}{15}\int_0^\infty dq\, q^2 C_1(q)\,. \tag{21}$$

We motivate our renormalization of the nonconvergent integral by comparing two expressions for the dielectric tensor of a suspension in an applied electric field. Our convergent mean field expression for the dielectric tensor[2] should be equivalent to the nonconvergent dielectric tensor of Onuki and Doi in the appropriate limits. The small $\beta$ limit of the mean field theory is equivalent to the small fluctuations is in the dielectric constant assumed by Onuki and Doi, while the long wavelength limit ($k \to 0$) of Onuki and Doi is equivalent to a static applied field assumed in the mean field theory. The material property $A$ can be evaluated, in the limit of small volume fraction, from the first order expression for dielectric constant, $\epsilon = \epsilon_1(1 + 3\beta\phi)$, to be $A = 9\beta^2 + O(\beta^3\phi)$. Expanding our mean field expression for the dielectric tensor to $O(\beta^2)$ yields

$$\frac{\epsilon_{\text{eff},z}}{\epsilon_1} = 1 + 3\beta\phi - 3\beta^2\phi^2 - \frac{18}{5}\beta^2\phi^2 \int_0^\infty \frac{1}{r} h_2(r)\, dr \tag{22}$$

while the small $k$ limit of Onuki and Doi is

$$\frac{\epsilon_{\text{eff},z}}{\epsilon_1} = \text{I.T.} + \frac{3}{5\pi^2}\beta^2\phi^2 \int_0^\infty q^2 h_2(q)\, dq\,. \tag{23}$$

Comparing the two equations, we equate the terms that depend on $h_2$ and thus find an equivalent real space expression of the nonconvergent integral in $q$ space

$$\int_0^\infty dq\, q^2 h_2(q) \equiv -6\pi^2 \int_0^\infty dr \frac{1}{r} h_2(r)\,. \tag{24}$$

The real space integral is convergent since $h_2(r) = O(1/r^3)$ for large $r$. We verify Eq. (24) in general by substituting the inverse Hankel transform of $h_i(q)$ for $h_i(q)$, and switching the order of integration to yield

$$\int_0^\infty dr \frac{1}{r} h_i(r) \equiv -\frac{1}{2\pi^2}\int_0^\infty dq\, q^2 h_i(q) \left[\int_0^\infty dr \frac{1}{r} j_2(qr)\right].$$

The integral over $r$ is tabulated[14], yielding

$$\int_0^\infty dr \frac{1}{r} h_i(r) \equiv -\frac{1}{6\pi^2}\int_0^\infty dq\, q^2 h_i(q)\,. \tag{25}$$

Thus Eq. (24) is valid for all Hankel transform pairs $h_i$.

Combining Eqs. (18), (20), and (21) yields a simple form for the dielectric tensor

$$\epsilon = \begin{pmatrix} \epsilon + \epsilon_{xx} & 0 & \epsilon_{xz} \\ 0 & \epsilon + \epsilon_{yy} & 0 \\ \epsilon_{xz} & 0 & \epsilon + \epsilon_{zz} \end{pmatrix}, \tag{26}$$

where

$$\epsilon_{xz} = \frac{\epsilon A \phi a^3}{24\pi}\left\{\int_0^\infty dq\, q^2 \times \left[\Psi_b\left(\frac{q}{2k}\right) - \frac{16}{15}\right]\rho h_+(q) - \frac{8}{45\pi^2}\int_0^\infty dr \frac{1}{r}\rho h_+(r)\right\}, \tag{27}$$

$$\epsilon_{xx} = \frac{\epsilon A \phi a^3}{24\pi}\left\{\int_0^\infty dq\, q^2 \times \left[\Psi_b\left(\frac{q}{2k}\right) - \frac{16}{15}\right]\rho h_2(q) - \frac{8}{45\pi^2}\int_0^\infty dr \frac{1}{r}\rho h_2(r)\right\}, \tag{28}$$

$\epsilon$ is the isotropic portion of the dielectric constant, $\epsilon_{xz}$ arises from the shear field, and $\epsilon_{xx} = \epsilon_{yy} = -\epsilon_{zz}/2$ all arise from the electric field.

With this renormalization for the nonconvergent integral in the dielectric tensor, we now determine the dichroism and the birefringence under combined shear and electric fields.

## V. BIREFRINGENCE AND DICHROISM

The birefringence and linear dichroism can be expressed in terms of the real and imaginary parts of the dielectric tensor, denoted respectively by $'$ and $''$. The two quantities are analogous; therefore, we will derive explicitly for the birefringence only and then write the corresponding results for dichroism. In the limit of zero electric field, the dichroism equation will reduce to that of Wagner *et al.*[7] The birefringence can be expressed in terms of the eigenvalues and eigenvectors of the real part of the dielectric tensor

$$\epsilon' = \begin{pmatrix} \epsilon + \epsilon'_{xx} & 0 & \epsilon'_{xz} \\ 0 & \epsilon + \epsilon'_{yy} & 0 \\ \epsilon'_{xz} & 0 & \epsilon + \epsilon'_{zz} \end{pmatrix}, \tag{29}$$

where the prime denotes the real part. Since the anisotropic terms are much smaller than the isotropic term and the index of refraction along each principal axis is the square root of the dielectric constant along that axis, the three principal refractive indices can be written as

$$n'_1 = n + \frac{1}{2n}\epsilon'_{yy}\,,$$
$$n'_2 = n + \frac{1}{2n}\left(-\frac{1}{2}\epsilon'_{xx} + \frac{1}{2}\sqrt{9\epsilon'^2_{xx} + 4\epsilon'^2_{xx}}\right), \tag{30}$$

and

$$n'_3 = n + \frac{1}{2n}\left(-\frac{1}{2}\epsilon'_{xx} - \frac{1}{2}\sqrt{9\epsilon'^2_{xx} + 4\epsilon'^2_{xx}}\right),$$

where $n = \sqrt{\epsilon}$, $n'_1$ is for the principal axis in the $y$ direction, and $n'_2$ and $n'_3$ are for orthogonal principal axes in the $xz$ plane. One principal axis is at the angle

$$\tan\theta_{\text{bi}} = -\frac{3\epsilon'_{xx}}{2\epsilon'_{xz}} + \sqrt{\left(\frac{3\epsilon'_{xx}}{2\epsilon'_{xz}}\right)^2 + 1} \tag{31}$$

while the second is at $\theta_{bi} + 90°$. For light propagating along the $y$ axis, the birefringence is

$$\Delta n' = n_2' - n_3' = \frac{1}{2n}\sqrt{9\epsilon_{xx}'^2 + 4\epsilon_{xz}'^2}\,. \tag{32}$$

The birefringence in the limit of pure electric field is $\Delta n_{el}' = 3\epsilon_{xx}/2n$, and for pure shear is $\Delta n_{sh}' = \epsilon_{xz}/n$, thus from Eqs. (18), (20) and (21),

$$\frac{\Delta n_{el}'}{nA} = \frac{\phi}{128\pi}\int_0^\infty dq\, q^2\left\{\mathrm{Re}\left[\Psi_b\left(\frac{q}{4ka}\right)\right] - \frac{16}{15}\right\}\rho h_2(q) - \frac{3}{10}\phi^2\int_0^\infty dr\frac{1}{r}h_2(r) \tag{33}$$

and

$$\frac{\Delta n_{sh}'}{nA} = \frac{\phi}{192\pi}\int_0^\infty dq\, q^2\left\{\mathrm{Re}\left[\Psi_b\left(\frac{\theta}{4ka}\right)\right] - \frac{16}{15}\right\}\rho h_+(q) - \frac{1}{5}\phi^2\int_0^\infty dr\frac{1}{r}h_+(r)\,. \tag{34}$$

In terms of the shear-induced and electric field-induced birefringence, the total induced birefringence is

$$\Delta n' = \sqrt{(\Delta n_{el}')^2 + (\Delta n_{sh}')^2}\,, \tag{35}$$

and the angle of the principal axis is

$$\tan\theta_{bi} = -\frac{\Delta n_{el}'}{\Delta n_{sh}'} + \sqrt{\left(\frac{\Delta n_{el}'}{\Delta n_{sh}'}\right)^2 + 1}\,. \tag{36}$$

Equation (35) does not necessarily recover the correct sign of the birefringence in the limits of pure shear or pure electric field, since Eq. (35) gives the absolute value of the birefringence in each of these two limits. The calculation of the birefringence in combined shear and electric fields must preserve the correct signs of the individual contributions, which modifies Eq. (35) to give

$$\Delta n' = \frac{\Delta n_{el}' + \Delta n_{sh}'}{|\Delta n_{el}' + \Delta n_{sh}'|}\sqrt{|(\Delta n_{el}'|\Delta n_{el}'| + \Delta n_{sh}'|\Delta n_{sh}'|)|}\,. \tag{37}$$

To first order, the electric field-induced birefringence of Eq. (33) is proportional to the dipole interaction strength $\Lambda$ via the Eq. (11) expansion of $h_2$, while the shear response of Eq. (34) scales with Pe via the first order expansion of $h_+$. In this linear response regime, the ratio of electric and shear induced birefringence is

$$\frac{\Delta n_{el}'}{\Delta n_{sh}'} = \frac{\Lambda(\Delta n_{el}')_{slope}}{\mathrm{Pe}(\Delta n_{sh}')_{slope}} = \frac{1}{\mathrm{Mn}}\frac{(\Delta n_{el}')_{slope}}{(\Delta n_{sh}')_{slope}}\,. \tag{38}$$

The two limiting slopes are fixed for given material properties, so the angles of the principal axes vary with the Mason number while the magnitude of the birefringence varies with $\Lambda$ and Pe separately. Because the limiting slopes are either positive or negative, depending on the the size of the particles, the angle of the principal axis varies either from 45° to 0° or from 45° to 90° as the structure changes from shear dominated to electric field dominated.

The dichroism equations are obtained from the imaginary part of the dielectric tensor, Eq. (26). All real parts, denoted by ′, become imaginary parts, denoted by ″, resulting in

$$\tan\theta_{di} = -\frac{\Delta n_{el}''}{\Delta n_{sh}''} + \sqrt{\left(\frac{\Delta n_{el}''}{\Delta n_{sh}''}\right)^2 + 1} \tag{39}$$

and

$$\Delta n = \frac{n_{el}'' + \Delta n_{sh}''}{|\Delta n_{el}'' + \Delta n_{sh}''|}\sqrt{|(\Delta n_{el}''|\Delta n_{el}''| + \Delta n_{sh}''|\Delta n_{sh}''|)|}\,, \tag{40}$$

where

$$\frac{\Delta n_{el}''}{nA} = \frac{\phi}{128\pi}\int_0^{4ka} dq\, q^2\,\mathrm{Im}\left[\Psi_b\left(\frac{q}{4ka}\right)\right]\rho h_2(q) \tag{41}$$

and

$$\frac{\Delta n_{sh}''}{nA} = \frac{\phi}{192\pi}\int_0^{4ka} dq\, q^2\,\mathrm{Im}\left[\Psi_b\left(\frac{\theta}{4ka}\right)\right]\rho h_+(q) \tag{42}$$

are the electric and shear field contributions to the dichroism. Note that the range of the dichroism integral is finite, 0 to $4ka$, because $\mathrm{Im}[\Psi_b(q/4ka)]$ is zero outside this range.[8] The small $q$ range makes the dichroism sensitive to the long range structure, and the upper limit enhances sensitivity to the particle size relative to the wavelength of light.

## VI. RESULTS

The magnitudes of both the dichroism and birefringence are sensitive to the size of particles relative to the wavelength of light. As shown in Figs. 2a and 2b, both magnitudes have a decaying oscillation when plotted vs particle size but are out of phase with one another. The positions of the birefringence and dichroism maxima move only slightly as $\phi$ increases $\phi = 0.1$ to 0.4. The magnitudes of birefringence and dichroism generally increase with volume fraction, but change order where the dichroism and birefringence are small, and for small particle sizes. For all four volume fractions the birefringence changes sign; this occurs over a small range of particle size for $\phi = 0.1$ and 0.2, and over a large range for $\phi = 0.3$ and 0.4. The dichroism changes sign for $\phi = 0.3$ and 0.4 over a small range of particle size. The sensitivity of birefringence and dichroism to particle size means that experimental interpretation is clouded by uncertainty in particle size and/or polydispersity. Given a monodisperse suspension, however, one can calculate a particle size from optical measurements over a range of wavelengths by matching the shapes of the experimental and theoretical curves.

The principal axes of birefringence and dichroism do not coincide since the relative magnitude of shear-induced to electric field-induced birefringence is not the same as the corresponding ratio for dichroism. In Fig. 3 the angles of the principal axes vary with the Mason number, where for large Mason number the shear field aligns the principal axes at 45°, and for small Mason number the electric field aligns the principal axes at 0°. When the reciprocal of the Mason number is $O(1)$ to $O(10)$ the dichroism and birefringence have widely differing principal axes, with the dichroism changing

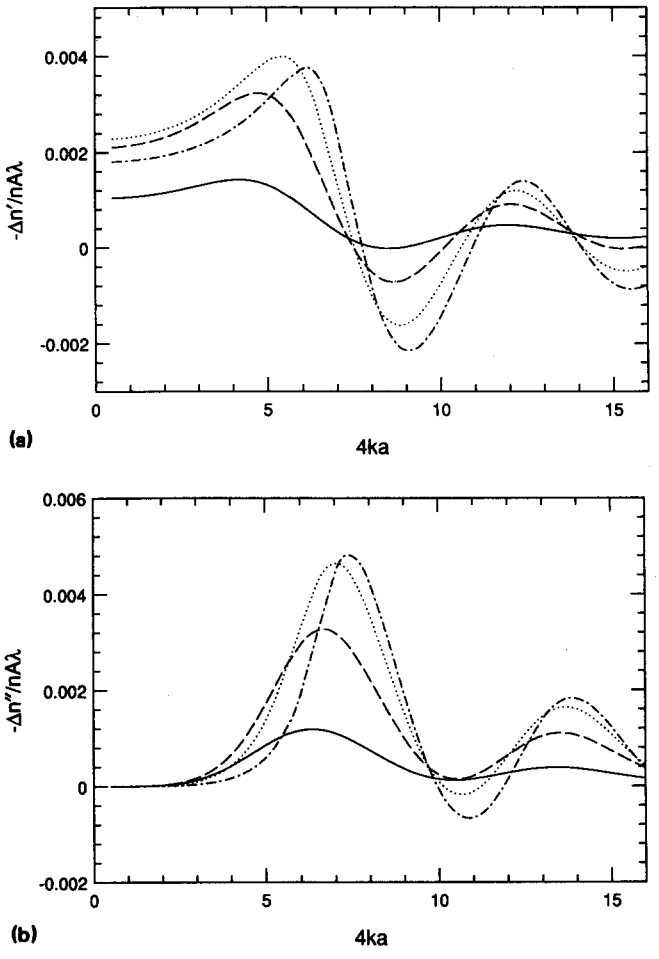


FIG. 2. Slopes of electric field-induced (a) birefringence and (b) dichroism vs the wave number of light $k$ and the particle size $a$ for volume fractions $\phi = 0.1$, 0.2, 0.3, and 0.4 (—, ---, ···, and ·–·–, respectively).

to an electric field orientation at lower field strengths than the birefringence.

The variation in the principal axes for dichroism and birefringence is further illustrated in Fig. 4 where $\theta_{bi}$ is plotted vs $\theta_{di}$ while the Mason number varies from electric field to shear field dominated. At low particle volume fractions

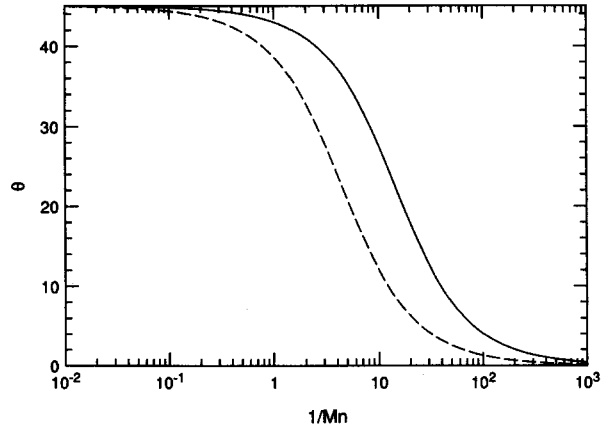


FIG. 3. Angles of principal axes of birefringence (—) and dichroism (---) vs the reciprocal of the Mason number, 1/Mn, for particle size $4ka = 5.0$ and volume fraction $\phi = 0.3$. Small Mn corresponds to electric field controlled structure; large Mn to shear controlled structure.

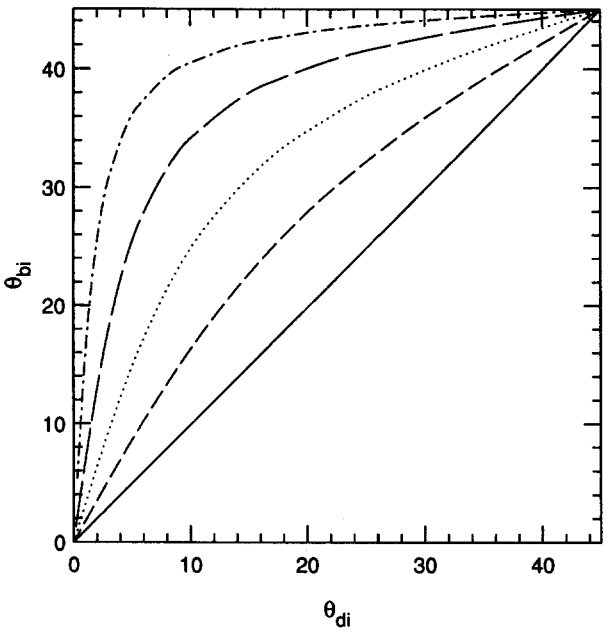


FIG. 4. Angles of principal axes of birefringes and dichroism for volume fractions $\phi = 0.1$, 0.2, 0.3, 0.4, and 0.5 (—, ---, ···, –·–, and ·–·–, respectively) and particle size $4ka = 5.0$.

the two angles become equal; conversely, increasing volume fraction increases the disparity between the angles. This disparity only arises when both shear and electric fields are important; in the limits of either pure shear or pure electric field, the two axes coincide.

We compare our predictions of dichroism and birefringence in an applied shear field to experiments by Wagner *et al.*[7] They experimentally determine the two optical properties and compare the dichroism with theoretical predictions using two different particle structure factors that include approximate hydrodynamic interactions. They did not compare birefringence to theory because of the nonconvergence of the birefringence integral.

Transmission electron microscopy (TEM) and dynamic light scattering (DLS) measurements gave particle radii of $a = 49 \pm 6$ and $70 \pm 7$ nm, respectively.[7] Radii of silica particles measured by TEM are significantly smaller than other methods, partly due to a 5% shrinkage in particle radius, observed by van Helden *et al.*,[15] apparently caused by radiation damage. Additional reasons for discrepancy include the following: (i) TEM radii are the number average over particle size, while the DLS radii are approximately the $Z$ average, and (ii) DLS measures hydrodynamic radius, which includes bound solvent, and so may exceed the true particle radius. These uncertainties in size impede comparison of theory and experiment.

A second source of experimental uncertainty is the determination of the material property of the suspension $A$ defined by Eq. (16). Wagner *et al.*[7] determine $A$ via differential refractometry and turbidity measurements. These two methods yield substantially different values for $A$. We employ the turbidity values, following the choice of Wager *et al.*,[7] to facilitate comparison with their results. This uncertainty in $A$ may contribute to discrepancies between theory and experiment.

TABLE I. Slope of low shear birefringence for particle volume fraction $\phi$, comparing experiments by Wagner *et al.* Ref. (7) with our renormalized equation for birefringence, employing the affine the affine deformation structure factor.

| | Slope of low shear birefringence $\times 10^{10}$ | | |
|---|---|---|---|
| $\phi$ | Experiment | Affine, $a = 50$ nm | Affine, a = 65 nm |
| 0.1 | 1.1 | − 2.94 | − 3.51 |
| 0.2 | − 2.8 | − 19.0 | − 20.7 |
| 0.3 | − 5.8 | − 85.8 | − 80.7 |
| 0.4 | − 27 | − 238 | − 211 |

TABLE II. Slope of low shear dichroism for particle volume fraction $\phi$, comparing experiments and theory of Wagner *et al.* Ref. (7) with predictions employing the affine deformation structure factor.

| | Slope of low shear dichroism $\times 10^{11}$ | | | |
|---|---|---|---|---|
| $\phi$ | Experiment | Wagner, $a = 50$ nm | Affine, $a = 50$ nm | Affine, $a = 65$ nm |
| 0.1 | − 2.4 | 0.68 | − 1.9 | − 6.5 |
| 0.2 | − 7.6 | 0.25 | − 3.1 | − 12.0 |
| 0.3 | − 8.8 | − 1.2 | − 2.9 | − 11.5 |
| 0.4 | − 6.2 | − 8.8 | − 1.6 | − 6.2 |

In Table I we compare the experimental birefringence with calculations employing our renormalized equation for birefringence, Eq. (34), where we employ the structure factor for affine deformation Eq. (10). We make theoretical predictions for two particle sizes $a = 50$ and 65 nm, which roughly correspond to the particle size as measured by TEM and DLS respectively. The predictions both exceed the experimental result by an order of magnitude. The experiment also has a change in sign in birefringence between volume fractions 0.1 and 0.2, while the calculations show a constant sign.

We compare the experimental dichroism with theoretical predictions in Fig. 5 and Table II. For particle radius of $a = 50$ nm, employing the affine deformation structure factor, predicted dichroism agrees with experiment at the lowest volume fraction $\phi = 0.1$, but then underpredicts the dichroism by a factor of three at the higher volume fractions. For $a = 65$ nm, the prediction agrees at the highest volume fraction $\phi = 0.4$, but overpredicts experiment at the lower volume fractions. The affine deformation structure factor predicts the correct sign as well as the maximum in the dichroism magnitude at intermediate volume fractions. Wagner *et al.*[7] predict the wrong sign for dichroism at $\phi = 0.1$, underpredict dichroism at lower volume fractions and slightly overpredict dichroism at $\phi = 0.4$, employing their particle structure factor with particle radius $a = 50$ nm.

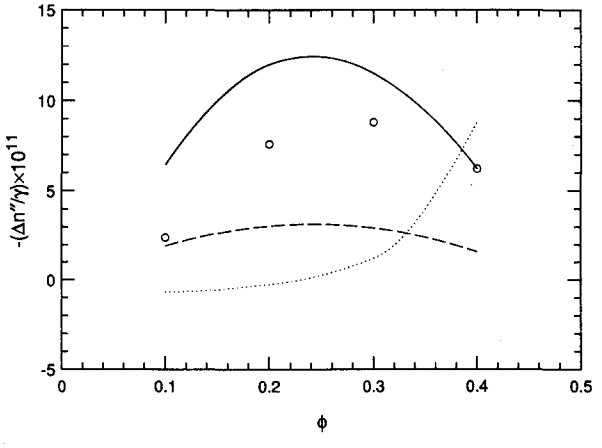


FIG. 5. Slope of low shear dichroism vs particle volume fraction $\phi$, comparing experiments by Wagner *et al.*[7] (○) with theoretical predictions employing the affine deformation structure factor, for particle radius $a = 50$ nm (—), $a = 65$ nm (---), and Wagner and Russel structure factor for $a = 50$ nm (···).

## VII. DISCUSSION

This study provides a framework to calculate birefringence and dichroism in external fields from a model of the structure factor. For combined electric and shear fields, both the angle of the principal axes and the magnitude of the birefringence and dichroism give insight into the microstructure of the suspension. Shear-induced structure has principal axes at 45° and 135°, while electric field-induced structure has principal axes at 0° and 90°. When both shear and electric fields are important the principal axes vary continuously between the two limits. As the fluid structure changes from shear to electric field dominated, the 45° principal axis will continuously change in angle toward either 0° or 90° principal axis of electric field induced structure. The direction of the shift depends on the relative signs of the shear-induced and electric field-induced optical properties.

Predictions of optical properties of suspensions in electric and shear fields allow comparison with experiments for the purpose of testing particle structure factors and to provide insight into experimental interpretation. Both the magnitudes and the orientation angles of birefringence and dichroism are sensitive to the choice of structure factors for electric field-induced and shear induced structure. Measurement of the principal axes of dichroism and birefringence in combined shear and electric fields is a particularly interesting experiment, since the orientation angles of the axes is a direct measure of the Mason number.

## ACKNOWLEDGMENTS

This work was supported in part by NSF under Grant No. CBT-8552495 and by IBM. We thank N. J. Wagner for providing us with a manuscript of Ref. 7, and G. G. Fuller and K. Smith for valuable discussions.

[1]W. B. Russel and A. P. Gast, J. Chem. Phys. **84**, 1815 (1986).
[2]P. M. Adriani and A. P. Gast, Phys. Fluids **31**, 2757 (1988).
[3]J. B. Hayter and R. Pynn, Phys. Rev. Lett. **49**, 1103 (1982).
[4]Z. P. Shulman, R. G. Gorodkin, E. V. Korobko, and V. K. Gleb, J. Non-Newt. Fluid Mech. **8**, (1981).

[5]B. J. Ackerson, C. G. De Kruif, N. J. Wagner, and W. B. Russel, J. Chem. Phys. **90**, 3250 (1989).
[6]B. J. Ackerson and P. N. Pusey, Phys. Rev. Lett. **61**, 1033 (1988).
[7]N. J. Wagner, G. G. Fuller, and W. B. Russel, J. Chem. Phys. **89**, 1580 (1988).
[8]A. Onuki and M. Doi, J. Chem. Phys. **85**, 1190 (1986).
[9]S. Hess, J. B. Hayter, and R. Pynn, Mol. Phys. **53**, 1527 (1984).
[10]N. J. Wagner and W. B. Russel, Physica A **155**, 475 (1989).
[11]G. Bossis and J. G. Brady, J. Chem. Phys. **91**, 1866 (1989).
[12]D. Ronis, Phys. Rev. Lett. **52**, 473 (1984).
[13]A. P. Gast and C. F. Zukowski, Adv. Colloid Interface Sci. (to be published).
[14]M. Abramowitz and I. A. Stegun, *Handbook of Mathematical Functions*, (Dover, New York, 1965), p. 486, 11.4.16.
[15]A. van Helden, J. Jansen, and A. Vrij, J. Colloid Interface Sci. **81**, 354 (1981).